Quantum Chemical Calculations (Ab Initio & DFT), Hirshfeld Surface Analysis, Crystal Structure and Molecular Docking Study of 2-Chloro-4-(4-fluoro-phenyl)-6-isopropyl-pyrimidine-5-carboxylic Acid Methyl Ester

Sahaj A. Gandhi, Urmila H. Patel, Rajesh D. Modh, Yogesh Naliyapara & Anil S. Patel

Journal of Chemical Crystallography

ISSN 1074-1542
Volume 46
Combined 10-12

J Chem Crystallogr (2016) 46:387-398
DOI 10.1007/s10870-016-0668-5

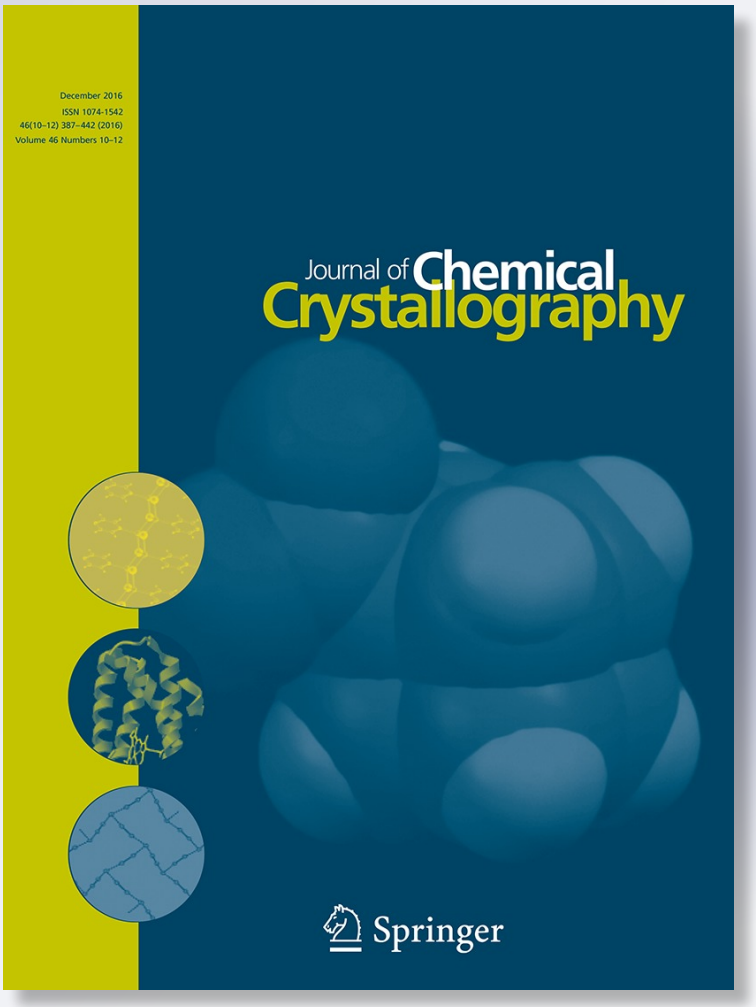

Springer

J Chem Crystallogr (2016) 46:387–398
DOI 10.1007/s10870-016-0668-5

ORIGINAL PAPER

Quantum Chemical Calculations (Ab Initio & DFT), Hirshfeld Surface Analysis, Crystal Structure and Molecular Docking Study of 2-Chloro-4-(4-fluoro-phenyl)-6-isopropyl-pyrimidine-5-carboxylic Acid Methyl Ester

Sahaj A. Gandhi[1] · Urmila H. Patel[2] · Rajesh D. Modh[3] · Yogesh Naliyapara[4] · Anil S. Patel[5]

Received: 3 June 2016 / Accepted: 23 September 2016 / Published online: 22 October 2016

Abstract Pyrimidine derivatives are well-known nitrogen containing heterocyclic compound which play an important role in medicinal and pharmaceutical applications. The synthesized compound, 2-chloro-4-(4-fluoro-phenyl)-6-isopropyl-pyrimidine-5-carboxylic acid methyl ester has been confirmed by single crystal X-ray diffraction studies. Title compound crystallizes in monoclinic space group $P2_1/c$ with $a = 8.5272(11)$ Å, $b = 17.774(2)$ Å, $c = 10.2732(14)$ Å, $\beta = 111.005(2)^\circ$ and $Z = 4$. The number of weak but significant C–H···O, C–H···N, C–F···π and π–π interactions take part, in the stability of the crystal packing and also the quantitative contributions of these interactions towards the crystal packing are investigated by Hirshfeld surface analysis. A static disorders have been observed in isopropyl substituent group of atoms C20 and C21 due to anisotropic thermal motion. Ab-initio and Density Functional Theory (DFT) calculations have been carried out for the title molecule using RHF/6-311G and B3LYP/6-311G basis set respectively without polarization function, predicting the optimized geometry which can well reproduce structural parameters. Mullikan charge distributions conforms the role of specific atom especially the donor/acceptor groups in the intermolecular interactions. In the present study, the neutral chlorine Cl (Mullikan charge is 0.0038 and 0.0256 by RHF and B3LYP respectively) does not take part in intermolecular interaction, whereas fluorine F (Mullikan charge is −0.4358 and −0.3319 by RHF and B3LYP respectively) took active part in intermolecular interactions. The calculated HOMO and LUMO energies show that charge transfer occur in the molecule. To investigate the effect of different substituted groups on molecular conformation and hence on its pharmacology, the title compound redesigned with different halogens replacing fluorine of fluoro-phenyl ring and docked with human estrogen receptor (2IOK) and attempted to predict the best drug.

Graphical Abstract The molecular structure of 2-chloro-4-(4-fluro-phenyl)-6-isopropyl-pyrimidine-5-carboxylic acid methyl ester has been determine, weak but significant interactions like C–H···O, C–H···F and π–π are involved in the stability of the structure and the quantitative contributions of these interactions towards the crystal packing are investigated by Hirshfeld surface analysis.

✉ Sahaj A. Gandhi
sahajg7@gmail.com

[1] Bhavan's Shri I. L. Pandya Arts–Science and Smt. J. M. Shah Commerce College, Dakor, Gujarat, India

[2] Department of Physics, Sardar Patel University, Vallabh Vidyanagar, Gujarat, India

[3] Gujarat Arts and Science College, Ahmedabad, Gujarat, India

[4] Department of Chemistry, Saurashtra University, Rajkot, Gujarat, India

[5] Department of Chemistry, Shree M. & N. Virani Science College, Rajkot, Gujarat, India

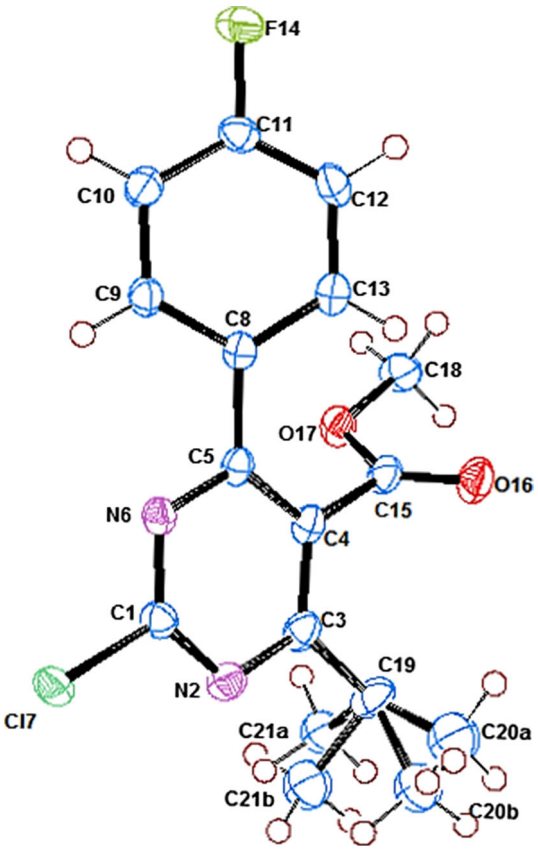

Keywords Pyrimidine derivative · Single crystal X-ray diffraction study · Hydrogen bond integrations · Ab-initio and DFT studies · Hirshfeld surface analysis · Molecular docking

Introduction

The derivatives of pyrimidine play vital role in many biological processes [1] and are present in nucleic acid, several vitamins, co-enzymes and uric acid. Some substituted pyrimidine and their derivatives have been reported to possess antimicrobial, antifungal, anti-cancer and antiviral activities [2–8]. The pyrimidine derivatives possesses dynamic role in the higher molar content polymers [9] and in the computation of torsional profiles as conjugated heterocyclic system [10]. The pyrimidine derivatives also show dynamic role in the higher molar content polymers [11]. As part of our ongoing research on X-ray crystallographic investigations of significant molecules [12–14], quantum chemical computational studies for the molecular structure have been carried out using Gaussian 09 software. Molecular conformations in the solid state and those in isolated state in the absence of weak intermolecular interactions are elucidated. The Hirshfeld surface analyses [15–17] represent a unique approach to investigate the intermolecular interactions in crystal packing. In this tool, the molecular surface provides a 'molecular fingerprint', a directly accessible 2D map which reveals the distribution of weak interactions like C–H, N–H, H–H etc. Analysis of intermolecular interactions using Hirshfeld surface provide a convenient means of quantifying the interactions within the crystal structure and offering considerable potential in crystal engineering. It is well documented that halogens on a specific drug molecule played a vital role in modify the drug activity. To investigate the role of different halogens on molecular conformations and hence on its activity, the title compound, redesigned with different halogens [Cl, Br and I] docked with human estrogen receptor and the docking score is investigated. The relative stability of the ligand receptor complexes are evaluated via docking study using molecular dynamics by HEX software.

Experimental Details

Synthesis Method

The synthetic route for the title compound is shown in Scheme 1. Initially, 3,4-dihydropyrimidine-2-(1H)-one (**I**) were synthesized by well-known multi-component Biginelli reaction of substituted benzaldehyde, methyl isobutyrate acetate and urea fusion at 150 °C in the presence of 2–3 drops of DMF as a catalyst. Thus obtained DHPM (**I**) were subjected the oxidative dehydrogenation using 60 % Conc. HNO_3 to furnish corresponding 2-hydroxypyrimidine (**II**) in excellent yield. The reaction of compound (**II**) treated with $POCl_3$ under reflux for 2 h afforded 2-chloropyrimidine derivative (**III**) up to 92 % yield.

*Methyl 4-(4-fluorophenyl)-6-isopropyl-2-oxo-1,2-dihydropyrimidine-5-carboxylate (**II**)*

White solid; R_f 0.48 (1:1 hexane–EtOAc); mp 180–182 °C; IR (KBr): 3470, 3093, 2999, 1735, 1648, 1586, 1450, 1261, 755, 700, cm^{-1}; ^1H NMR (300 MHz, $CDCl_3$): δ 1.14–1.16 (d, 6H, 2 × $^i prCH_3$), 3.06–3.11 (m, 1H, $^i prCH$), 3.54 (s, 3H, OCH_3), 6.92–6.98 (t, 2H, Ar–H), 7.29–7.40 (d, 2H, Ar–H), 8.0 (s, 1H, NH); ^{13}C NMR (DEPT):(75 MHz, $CDCl_3$): 20.82, 31.98, 52.28, 115.28, 115.56, 129.82, 129.93; MS (*m/z*): 291 (M^+).

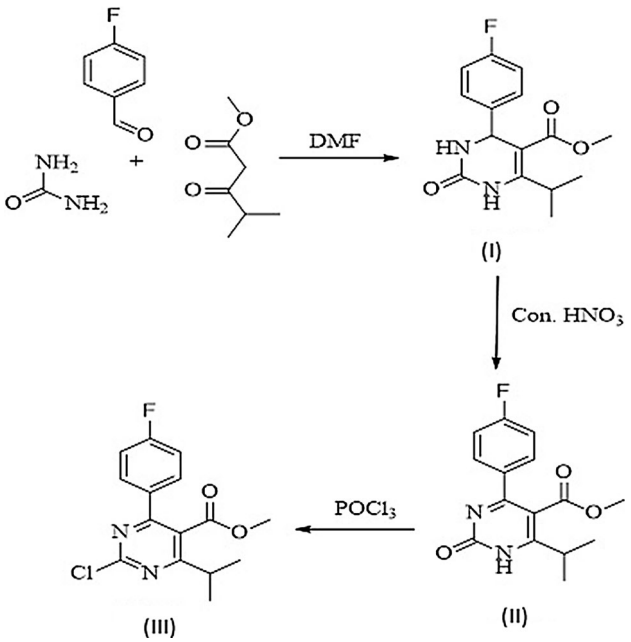

Scheme 1 Synthesis of 2-chloro-4-(4-fluro-phenyl)-6-isopropyl-pyrimidine-5-carboxylic acid methyl ester

*2-Chloro-4-(4-fluoro-phenyl)-6-isopropyl-pyrimidine-5-carboxylic acid methyl ester (**III**)*

White solid; R_f 0.83 (8:2 hexane–EtOAc); mp 130–132 °C; IR (KBr): 3057, 3034, 2972, 2931, 2872, 1828, 1726, 1687, 1572, 1541, 871, 767, 730, 702 cm^{-1}; ^1H NMR (500 MHz, DMSO): δ 1.25–1.26 (d, 6H, 2 × $^{i}prCH_3$), 3.10–3.16 (m, 1H, $^{i}prCH$), 3.75 (s, 3H, OCH_3), 6.97–6.99 (d, 2H, Ar–H), 7.50–7.52 (d, 2H, Ar–H); ^{13}C NMR (125 MHz, DMSO): 21.40, 30.04, 53.22, 123.34, 128.07, 128.95, 131.07, 135.59, 160.21, 165.50, 167.00, 176.04; MS (*m/z*): 309 (M^+).

Thin-layer chromatography was accomplished on 0.2-mm precoated plates of silica gel G60 F_{254} (Merck). Visualization was made with UV light (254 and 365 nm) or with an iodine vapor. IR spectra were recorded on a FTIR-8400 spectrophotometer. ^1H (300 MHz) and (500 MHz) and ^{13}C (75 MHz) and (125 MHz) NMR spectra were recorded on a Bruker AVANCE II spectrometer in $CDCl_3$ and DMSO. Chemical shifts are expressed in δ ppm downfield from TMS as an internal standard. Mass spectra

Table 1 Crystal data and experimental details

Empirical formula	C_{15} H_{14} Cl F N_2 O_2
Formula weight	308.73
Temperature	296(2) K
Wavelength (λ)	0.71073 Å
Crystal system	Monoclinic
Space group	$P2_1/c$
a	8.5272(11) Å
b	17.774(2) Å
c	10.2732(14) Å
β	111.005(2)°
Volume (V)	1453.6(3) $Å^3$
Z	4
Density (ρ)	1.411 Mg/m^3
Absorption coefficient (μ)	0.279 mm^{-1}
F(000)	640
Crystal shape and color	Needle, White
Crystal size	0.24 × 0.13 × 0.09
θ range for data collection (°)	2.29–28.27
Index ranges	$-11 \le h \le 10$; $-21 \le k \le 23$; $-8 \le l \le 13$
Reflections collected	7126
Independent reflections	3317
Absorption correction	None
Refinement method	Full-matrix least-squares on F^2
Data/restraints/parameters	3317/0/190
Calculated weights, *w*	$w = 1/[\sigma^2(Fo^2) + (0.0773P)^2 + 0.974P]$ where $P = (Fo^2 + 2Fc^2)/3$
Goodness-of-fit on F^2	1.065
Final *R* indices [$I \ge 2\sigma(I)$]	$R_1 = 0.0613$, $wR_2 = 0.193$
Largest diff. peak and hole	0.908 and −0.653

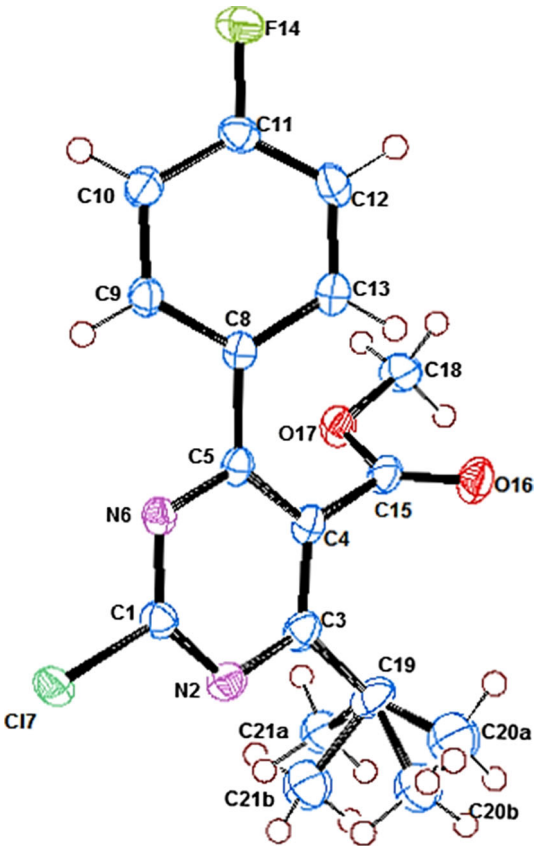

Fig. 1 The ORTEP view of the title molecule (**III**) shows atomic labelling scheme and 50 % probability level displacement ellipsoids

Table 2 Bond lengths (Å), bond angles (°) and torsional angles (°) involving non-hydrogen atoms by X-ray data (with estimated standard deviation in parentheses) and by theoretical calculations at the RHF/6-311G and B3LYP/6-311G levels of theory

Bond lengths (Å)	X-ray	RHF/6-311G	B3LYP/6- 311G
C1–N2	1.324 (3)	1.3084	1.3255
C1–N6	1.313 (3)	1.3111	1.3248
C1–Cl7	1.741 (2)	1.7792	1.8168
C3–N2	1.348 (3)	1.3401	1.3583
C3–C4	1.393 (3)	1.3964	1.4110
C3–C19	1.518 (3)	1.5130	1.5156
C4–C5	1.408 (3)	1.3982	1.4143
C4–C15	1.507 (3)	1.4834	1.4878
C5–N6	1.352 (3)	1.3385	1.3603
C5–C8	1.479 (3)	1.4803	1.4785
C8–C9	1.397 (3)	1.3917	1.4064
C8–C13	1.398 (3)	1.3928	1.4066
C9–C10	1.383 (3)	1.3855	1.3945
C10–C11	1.377 (3)	1.3738	1.3866
C11–F14	1.359 (3)	1.3724	1.3983
C11–C12	1.375 (3)	1.3754	1.3874
C12–C13	1.383 (3)	1.3833	1.3928

Table 2 continued

Bond lengths (Å)	X-ray	RHF/6-311G	B3LYP/6- 311G
C15–O16	1.204 (3)	1.2122	1.2361
C15–O17	1.327 (3)	1.3342	1.3678
C18–O17	1.457 (3)	1.4463	1.4735
C19–C20a	1.392 (8)	1.5381	1.5474
C19–C20b	1.563 (5)		
C19–C21a	1.451 (5)	1.5340	1.5420
C19–C21b	1.630 (7)		
Bond angles (°)	**X-ray**	**RHF/6-311G**	**B3LYP/6-311G**
N2–C1–N6	129.6 (2)	126.25	127.33
N2–C1–Cl7	115.2(2)	117.01	116.42
N6–C1–Cl7	115.2 (2)	116.74	116.24
C1–N2–C3	115.0 (2)	117.96	117.38
N2–C3–C4	121.1 (2)	119.56	119.87
N2–C3–C19	115.5 (2)	115.62	115.46
C4–C3–C19	123.3 (2)	124.82	124.67
C3–C4–C5	118.4 (2)	118.00	118.20
C3–C4–C15	119.7 (2)	120.24	119.85
C5–C4–C15	121.9 (2)	121.75	121.95
N6–C5–C4	119.6 (2)	119.84	119.68
N6–C5–C8	115.2 (2)	115.27	115.18
C4–C5–C8	125.1 (2)	124.88	125.12
C1–N6–C5	116.1(2)	118.29	117.33
C9–C8–C13	118.5 (2)	119.09	118.94
C9–C8–C5	122.3 (2)	121.64	121.95
C13–C8–C5	119.1 (2)	119.23	119.05
C10–C9–C8	120.9 (2)	120.66	120.68
C11–C10–C9	118.2 (2)	118.24	118.32
F14–C11–C12	118.9 (2)	118.53	118.51
F14–C11–C10	117.8 (2)	118.57	118.63
C12–C11–C10	123.2 (2)	122.90	122.86
C11–C12–C13	117.7 (2)	118.32	118.32
C12–C13–C8	121.4 (2)	120.63	120.74
O16–C15–O17	125.4 (2)	122.69	123.09
O16–C15–C4	124.5 (2)	124.93	125.58
O17–C15–C4	110.1 (2)	112.37	111.31
C15–O17–C18	115.5 (2)	119.86	117.18
C21a–C19–C20b	113.7 (5)	111.57	111.41
C21b–C19–C20a	112.1(5)		
C3–C19–C20a	112.8 (4)	111.10	111.09
C3–C19–C20b	110.6 (3)		
C3–C19–C21a	110.1 (3)	109.42	109.30
C3–C19–C21b	109.6 (3)		

Torsional Angles (°)	X-ray	RHF/6-311G	B3LYP/6-311G
Cl7–C1–N2–C3	−178.65 (17)	−176.35	−177.98
N2–C3–C4–C5	−2.1 (3)	−3.46	−2.32
C19–C3–C4–C15	−3.7 (4)	−3.83	−3.01

Table 2 continued

Torsional Angles (°)	X-ray	RHF/6-311G	B3LYP/6-311G
C4–C5–C8–C9	28.4 (3)	34.69	40.99
C3–C4–C15–O16	66.6 (3)	59.79	60.66
C3–C4–C15–O17	−113.1 (2)	−118.74	−118.16
O16–C15–O17–C18	4.8 (3)	3.01	3.54
C4–C15–O17–C18	−175.55 (19)	−178.4265	−177.61
C4–C3–C19–C20a	97.3 (5)	−107.5808	−106.02
C4–C3–C19–C20b	130.2 (3)		
C4–C3–C19–C21a	−103.3 (3)	129.0724	130.34
C4–C3–C19–C21b	−137.1 (4)		

were determined using direct inlet probe on a GCMS-QP 2010 mass spectrometer (Shimadzu). Solvents were evaporated with a BUCHI rotary evaporator. Melting points were measured in open capillaries and are uncorrected.

Crystal Growth

The synthesized title molecule (**III**), 2-chloro-4-(4-fluorophenyl)-6-isopropyl-pyrimidine-5-carboxylic acid methyl ester, in the pure powder form was soluble in methanol, ethanol and ethyl acetate etc. Transparent white needle shaped diffraction quality single crystals were grown by slow evaporation technique using ethanol solvent.

X-Ray Diffraction Study

A suitable sample of single crystal of size (0.24 × 0.13 × 0.09) mm^3 was selected for the crystallographic study. Three dimensional X-ray intensity data were collected from a crystal for θ ranging from 2.29° to 28.27° using scan mode on CCD diffractometer (Bruker smart Apex-II) with graphite monochromated MoKα radiation of wavelength 0.71073 Å. The cell refinement and data reductions are performed using SAINT programme. In total, 7126 reflections have been collected for *hkl* ranging $-11 \leq h \leq 10$, $-21 \leq k \leq 23$ and $-8 \leq l \leq 13$, out of which 2839 reflections found to satisfy the criteria $I > 2(I)$ and used for further structure solution and refinement purpose. The structure was solved by the direct method using SHELXS-97 [18] and was refined by full matrix least squares based on F^2 using SHELXL-2016 [19]. The molecular graphic were drawn using the ORTEP-3 for Windows [20] and PLATON programs [21]. All non-hydrogen atoms are refined anisotropically. The structure is refined to $R = 0.0600$ for the observed reflections 3317 and $R = 0.1617$ for all data, Goodness of fit $S = 1.065$. Highest and lowest electron density peaks '$\Delta\rho$' are 0.907 and −0.653 $eÅ^{-3}$ respectively. CCDC 1003686 contains the supplementary crystallographic data for the compound. These data can be obtained free of charge via http://www.ccdc.cam.ac.uk/conts/retrieving.html, or from the Cambridge Crystallographic Data Centre, 12 Union Road, Cambridge CB2 1EZ, UK; fax: (þ44) 1223-336-033; or e-mail: deposit@ccdc.cam.ac.uk. Preliminary crystallographic data and details of

Table 3 Intra and intermolecular hydrogen bond interactions (distances in Å, angles in °)

D–H···A	d(D–H) (Å)	d (D–A) (Å)		d (H–A) (Å)		(D–H···A)°	
Hydrogen bond interactions							
C9–H9···O16 (i)	0.93	3.437(3)		2.634(2)		145.07(17)	
C19–H19···O16 (i)	0.98	3.190(4)		2.458(2)		131.27(18)	
C9–H9···O16 (iii)	0.93	3.374(4)		2.789(2)		121.90(17)	
C10–H10···O16 (iii)	0.93	3.357(4)		2.767(2)		122.31(18)	
C18–H183···O16 (iii)	0.96	3.592(4)		2.669(2)		161.29(18)	
C18–H181···N6 (iv)	0.96	3.525(4)		2.630(2)		155.24(19)	
C21–H212···O17 (v)	0.96	3.427(7)		2.792(2)		124.37(36)	
π–π interaction							
Cg(I)–Cg(J)	Cg(I)···Cg(J)Å	α	β	γ	Cg(I)···P Å		Cg(J)···P Å
1–2 (ii)	3.9554(16)	28.53	16.84	28.20	3.486		3.786
C–F···π interaction							
C–F(I)···Cg(J)	d(F–Cg) Å	d(C–Cg) Å		C–F···Cg °	γ°		F···P Å
C8–F1···Cg(1) (ii)	3.971(5)	3.900(2)		71.42(13)	26.78		3.482

Symmetry code: (i) *x*, *y*, *z*; (ii) 2−*x*, −*y*, 1−*z*; (iii) $-x+1, -y+1, -z+2$; (iv) $x-1, +y, +z$; (v) $-x+1, -y+1, -z+1$

Cg (1) and Cg(2) represents the centroid of the rings (N1,N2,C1,C2,C3,C4) and (C5–C6–C7–C8–C9–C10) respectively

the data collection along with structure refinement parameters are listed in Table 1.

Computational Details

The quantum chemical study of the title compound has been performed within the framework of Hartree–Fock [22] and the density functional theory with Becke's three-parameter hybrid exchange functional with Lee–Yang–Parr correlation functional (B3LYP) employing 6-311G basis set [23, 24]. All quantum chemical calculations are performed using computer software Gaussian-09 [25] and Gauss –View molecular visualization program [26]. The RHF and B3LYP (Becke three parameter Lee–Yang–Parr) method with 6-311G* basis set are used to determine optimized geometry in which bond lengths, bond angles, torsional angles and dihedral angles are calculated and compared with those of the experimental data (X-ray). The optimization algorithm included in Gaussian is the "Berny algorithm" developed by Bernhard Schlegel. This algorithm uses the forces acting on the atoms of a given structure together with the second derivative matrix to predict energetically more favorable structures and thus optimize the molecular structure towards the next local minimum on the potential energy surface. An explicit calculation of the second derivative matrix is quite costly, the Berny algorithm constructs an approximate Hessian at the beginning of the optimization procedure through application of a simple valence force field, and then uses the energies and first derivatives calculated along the optimization pathway to update this approximate Hessian matrix. Hirshfeld surface of the title molecule has been

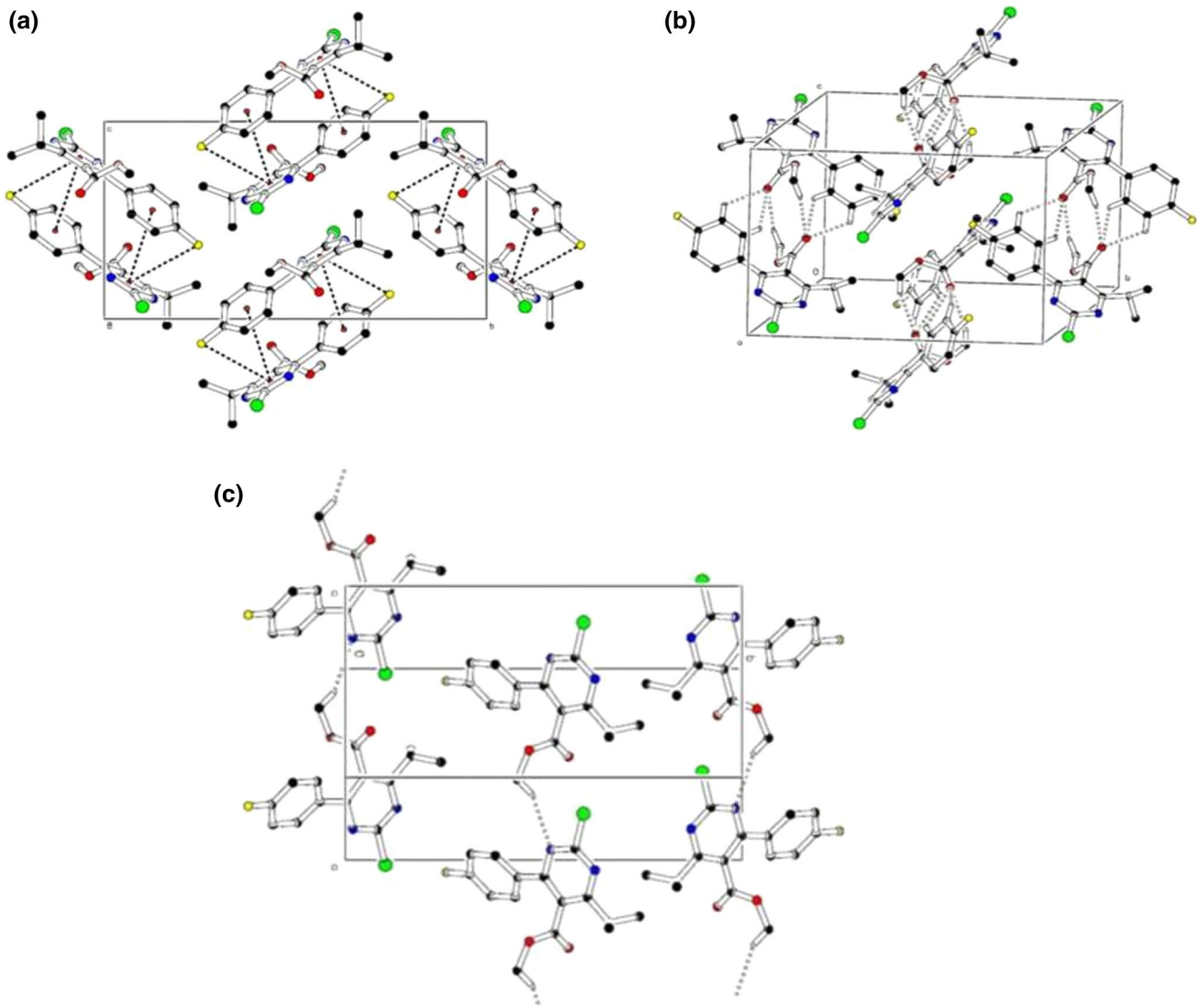

Fig. 2 The molecular packing diagram showing **a** C–F···π and π–π interactions, for the sake of clarity H atoms have been omitted **b** C–H···O hydrogen bond interactions **c** C–H···N interactions

calculated using CRYSTALEXPLORER 2.1 [27, 28]. The docking experiments are performed using the docking software Hex which works on FFT correlation using spherical polar coordinates [29].

Results and Discussion

X-Ray Crystallography

The ORTEP diagram of the title compound, 2-chloro-4-(4-fluoro-phenyl)-6-isopropyl-pyrimidine-5-carboxylic acid methyl ester with thermal ellipsoids drawn at a 50 % probability is shown in Fig. 1. The title compound shows static disorder at C20 and C21 atoms. Atoms C20 and C21 are refined as disordered over two partially occupied positions, with an occupancy ratio of 0.417(8) and 0.583(8). Bond lengths, bond angles and torsional angles about few significant bonds involving non-hydrogen atoms as obtained by X-ray data (with estimated standard deviation in parentheses) and by theoretical at the RHF/6-311G and B3LYP/6-311G levels of theory are summarized in Table 2. The pyrimidine ring and fluoro-phenyl ring are planar and the dihedral angle between them is 28.53(13)°. Intra molecular weak C9–H9···O16 and C19–H19···O17 hydrogen bond interactions led to the formation of pseudo seven and six membered hydrogen-bond pattern with graph set motif S(7) and S(6), thus locking the molecular conformation and eliminating conformational flexibility.

Intermolecular interactions such as C–H···O and C–H···N are weaker in the hydrogen bond hierarchy and are of secondary importance in directing the supramolecular assembly. The crystal packing is governed by diverse set of weak but significant C–H···O, C–H···N, C–F···π and π–π interactions, play an important role in stabilization of supramolecular aggregation. All the geometrical calculations are performed using PLATON and PARST [30] software. The Intra and intermolecular hydrogen bond interactions geometry are summarized in Table 3.

The directional specific $\pi\cdots\pi$ interactions involving inversely related the centroids of pyrimidine ring and that fluoro-phenyl ring at $2-x$, $-y$, $1-z$ forms stacking interactions as seen on *bc* plane (Fig. 2a). The Cg–Cg distance between two centroids is 3.9554(16) Å and the angle α between these two planes is 28.53°. In addition, a significant C–F···π interaction contributes to the molecular packing where the fluorine of fluoro-phenyl ring via C11–F14 linked

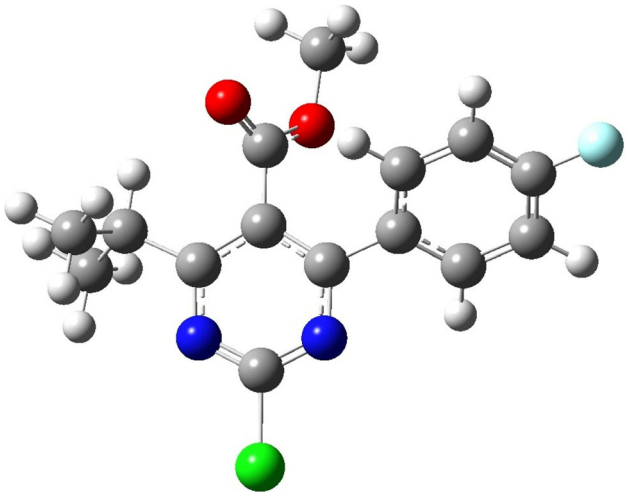

Fig. 4 Optimized geometry of the title compound using B3LYP method

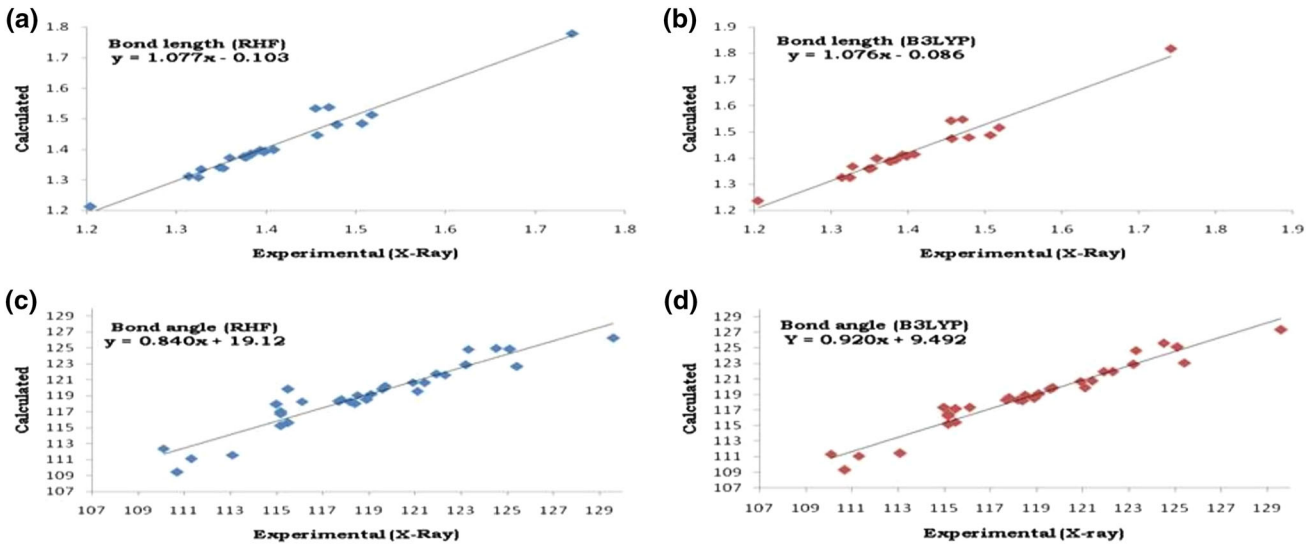

Fig. 3 Correlation of calculated and experimental bond lengths and bond angles

to the centroid of inversely related pyrimidine ring at $2-x$, $-y$, $1-z$, with C11–F14···Cg(1) (ii) = 3.900(2) Å. In the crystal packing, carbon atoms of the floro-phenyl ring C9 via H9 and C10 via H10 act as potential donor to oxygen atom O16 of carboxylic acid; C9–H9···O16 and C10–H10···O16 interactions at $(-x+1, -y+1, -z+2)$ generate a graph set motif $R_2^1(5)$ [31]. Further the carbon atom C18 of carboxylic acid acts as a donor to the same molecule $(-x+1,-y+1,-z+2)$ of oxygen atom O16 via H183 and generate a ring of graph set motif $R_2^2(10)$ as shown in Fig. 2b. Here the oxygen atom O16 works as trifurcated accepter in C–H···O hydrogen bond interactions. The carboxylic acid atom C21 at (x, y, z) acts as a donor via atom H212, to accepter atom O17 of carboxylic acid at $(-x+1,-y+1,-z+1)$ generating a ring of $R_2^2(16)$ graph set motif at each inversion center. Figure 2c illustrates that carbon C18 of carboxylic acid acts as donor to nitrogen atom N6 of $x-1, +y, +z$ molecule, C18–H181…N6 hydrogen bond interactions generated a chain parallel to a-axis.

Ab-Initio and DFT Studies

Geometry Optimization Calculations

The ab initio and Density Functional Theory (DFT) with Gaussian-09 program package employing B3LYP (Becke three parameter Lee–Yang–Parr) method with 6-311G basis set is used to determine optimized structure. Selected bond lengths, bond angles and torsional angles compared with those of the experimental data and are presented in Table 2. The graphical representation of correlation between experimental versus theoretical bond lengths using RHF and B3LYP methods are depicted in Fig. 3a, b and those for the bond angles are displayed in Fig. 3c, d, respectively. The highest bond length difference is 0.079 and 0.087 Å for the C19–C21 bond at RHF and B3LYP respectively, whereas the biggest bond angle deviation occurred in the C15–O17–C18 angle (4.3555°) in RHF method and C1–N2–C3 angle (2.3177°) in B3LYP method. These observed changes in optimized geometry with those of X-ray data are due to thermal motion of the atoms and also adopting atomic scattering factors for the isolated (spherical) atom in the X-ray refinement [32]. The correlation coefficient in bond lengths by RHF and B3LYP are 0.9776 and 0.9732 respectively. The root mean square error (RMSE) is found to be about 0.0252 Å for RHF and 0.0340 Å for B3LYP, indicating that the bond lengths obtained by the HF method shows the strongest correlations with the experimental values. The root mean square errors for bond angles are 1.5455° and 1.0755° RHF and B3LYP respectively. The correlation coefficient in bond angles by RHF and B3LYP are 0.9414 and 0.9713 respectively. The optimized geometry of molecule obtained by B3LYP method is shown in Fig. 4.

Table 4 Mulliken charges (*e*) for the title compound

Atom	Calculated (RHF)	Calculated (B3LYP)	Atom	Calculated (RHF)	Calculated (B3LYP)
C1	0.2352	0.0830	H9	0.2187	0.2022
N2	−0.4423	−0.2839	H10	0.2050	0.1861
C3	0.3756	0.2267	H12	0.2061	0.1882
C4	−0.0843	0.0320	H13	0.2106	0.1943
C5	0.1996	0.0495	H181	0.1974	0.2065
N6	−0.4524	−0.2960	H182	0.1969	0.2037
Cl7	0.0037	0.0255	H183	0.1939	0.2018
C8	0.0098	−0.0107	H19	0.2035	0.2013
C9	−0.0950	−0.0526	H201	0.1779	0.1824
C10	−0.2379	−0.2258	H202	0.1926	0.1910
C11	0.4233	0.3294	H203	0.1962	0.1992
C12	−0.2189	−0.2005	H211	0.2074	0.2077
C13	−0.0815	−0.0603	H212	0.1691	0.1748
F14	−0.4358	−0.3319	H213	0.1733	0.1775
C15	0.6136	0.3642			
O16	−0.5140	−0.3797			
O17	−0.6291	−0.4536			
C18	−0.1727	−0.2679			
C19	−0.3094	−0.2768			
C20	−0.4724	−0.4958			
C21	−0.4642	−0.4914			

Mulliken Charge Distributions

The atomic charge values obtained by the Mulliken population analysis using RHF and B3LYP methods with 6-311G level without polarization function are tabulated in Table 4. It may be noted that the all oxygen and nitrogen atoms have negative charge and all hydrogen atoms have positive charge. The charge of oxygen O17 atom has more negative than oxygen O16 and nitrogen atom N6 has more negative charge against N2 nitrogen atom. Among the halogen atoms, the chlorine atom Cl7 is almost neutral (0.0037 for RHF and 0.0255 for B3LYP) whereas fluorine atom F14 contain negative charge (−0.4358 for RHF and −0.3319 for B3LYP). Being neutral, chlorine atom does not take part in any intra and intermolecular hydrogen bond interactions, whereas the fluorine atom takes part in C–F···Π hydrogen bond interactions, which supports the X-ray data (Table 3). The carbon atoms C11 and C15 are more positive and C20 and C21 are more negative than the other carbon atoms in the title molecule. The Mulliken charge distributions graphically plotted using RHF and B3LYP methods are shown in Fig. 5a, b respectively.

HOMO and LUMO Analysis

Table 5 is the data for HOMO and LUMO energies calculated using RHF and B3LYP methods and Fig. 6 is the plot for B3LYP/6-311G method. The dipole moment is the

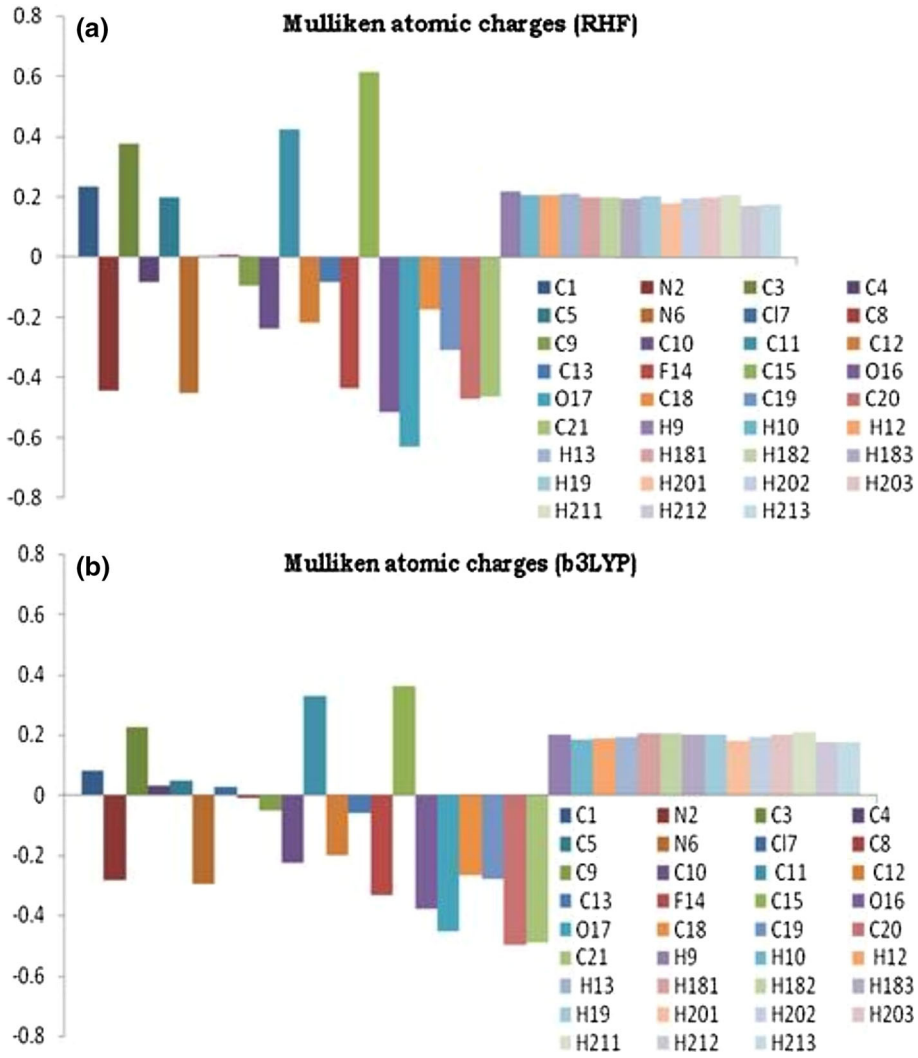

Fig. 5 Graph sheets of Mulliken charges (*e*) for the title compound

Table 5 Homo–Lumo, total energy and dipole moment of the title compound

Method	HOMO	LUMO	Energy band gap	Total energy (Hartree)	Dipole moment (Debye)
RHF	−0.35,662	0.05,144	−0.40,806	−1393.3352	4.2899
B3LYP	−0.26,983	−0.09,031	−0.17,952	−1399.7658	4.2825

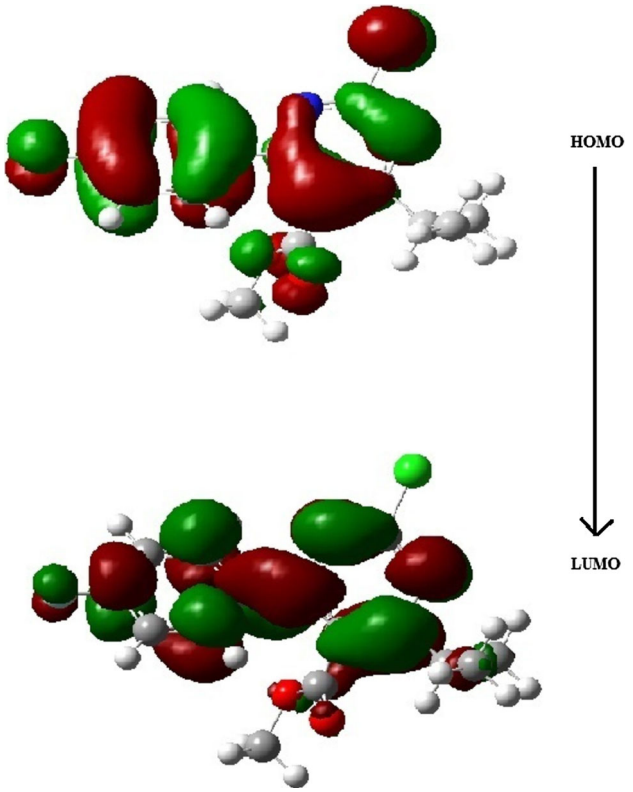

Fig. 6 Highest occupied molecular orbital (*HOMO*) and the lowest unoccupied molecular orbital (*LUMO*)

measure of the asymmetry in the molecular charge distributions of the compound. The high value suggests that the title compound is reactive and attractive for further interactions with other system [33]. Figure 6 shows that HOMO and LUMO delocalized on the pyrimidine ring. The calculated energy value of HOMO is −0.26983 eV and LUMO is 0.05144 eV. Analysis of the wave function indicates that the electron absorption corresponds to the transition from the ground state to the first exited state and is mainly described by electron excitation from the highest occupied molecular orbital (HOMO) to the lowest unoccupied molecular orbital (LUMO). The energy gap of HOMO–LUMO explains the charge transfer interaction within the molecule [34].

Hirshfeld Surface Analyses

The Hirshfeld surfaces and the associated 2D fingerprint plots calculated using Crystal Explorer software. The number of significant interactions like C–H···O and C–H···N (Table 3) can be seen in the Hirshfeld surface as the bright red areas Fig. 7a shows surfaces those have been mapped over dnorm range 0.5–1.5 Å. Figure 7b, c are the shape index, ranging from −1.0 to 1.0 Å and curvedness ranging from 4.10 to 0.48 Å respectively. The light red spots are due to C–H···O and C–H···N interactions. Figure 8 is the 2D fingerprint plots indicating the quantitative contributions of intermolecular contacts to the Hirshfeld surfaces, H···H (34.4 %, Fig. 8a), Cl···H (14.4 %, Fig. 8b), C···H (12.5 %, Fig. 8c), O···H (10.7 %, Fig. 8d), F···H (9.9 %, Fig. 8e) and N···H (6.9 %, Fig. 8f). In addition the very weak but significant C···C interaction is contributes 3.6 % towards the total Hirshfeld surface. Complementary regions are visible in the fingerprint plots where one molecule acts as donor ($de > di$) and the other as an acceptor ($de < di$). The nature of interactions of the title compound is more easily understood using Hirshfeld surfaces, highlighting the power of the technique in mapping out the interactions.

Molecular Docking Using HEX Software

In the present work, to investigate the role of halogens, the title compound redesigned with different substituted halogens (Fig. 9a), is docked with human estrogen receptor (2IOK, Fig. 9b). The energy values obtained by docking study are tabulated in Table 6 revealing the best ligand structure fitting is due to iodine compare to other halogens. Figure 9c displays the docking between the ligand with

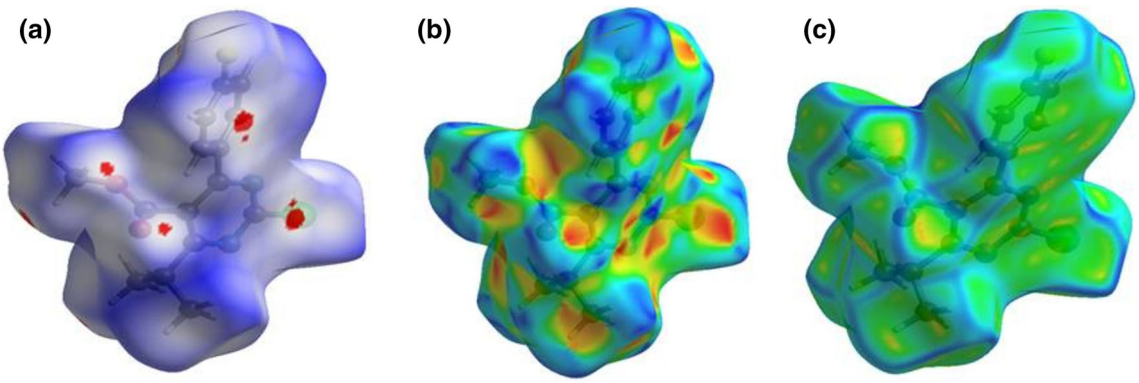

Fig. 7 Hirshfeld surfaces mapped with **a** dnorm, **b** shape index and **c** curvedness of the title compound

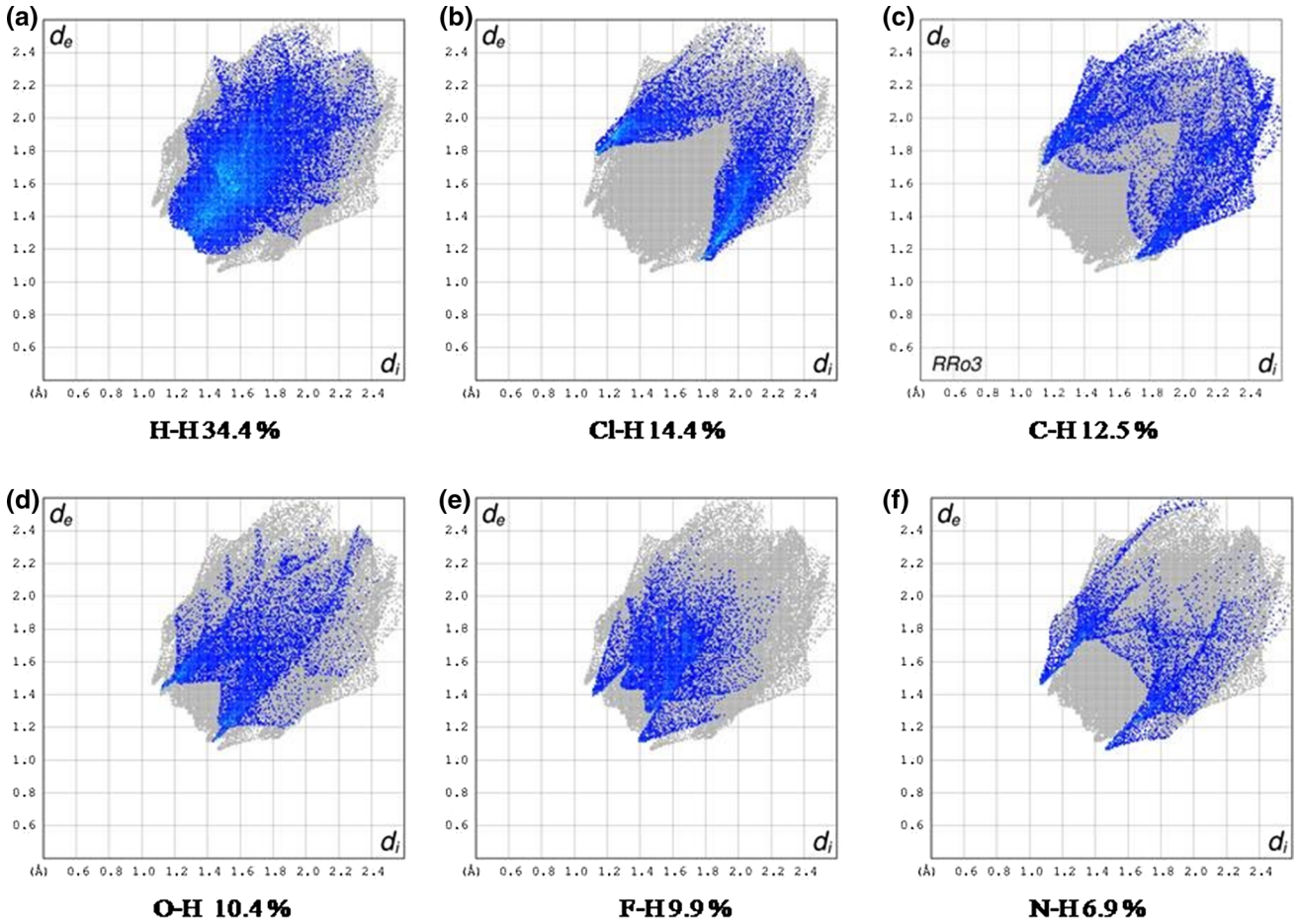

Fig. 8 Fingerprint plot of resolved into H–H, Cl–H, C–H, F–H, N–H and F–Cl contacts showing the percentages of contacts contributed to the total Hirshfeld surface area of molecule

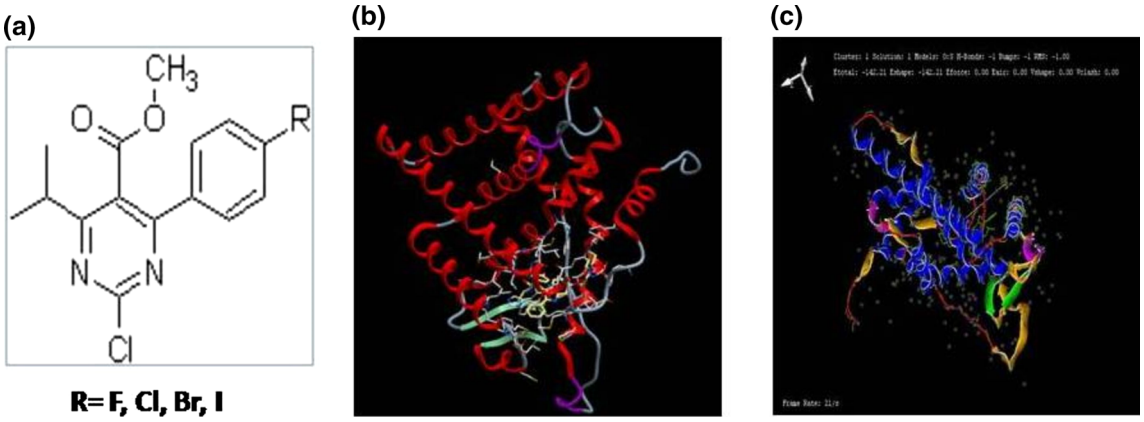

Fig. 9 **a** Structure of compound with different R group. **b** The structure of human estrogen receptor. **c** Docking interaction and binding energy of human estrogen receptor with compound I derivative

Table 6 Docking results of the compounds and receptor (2IOK)

Compound	*E*-value
R1 (F)	−134.94
R2 (Cl)	−118.08
R3 (Br)	−138.01
R4 (I)	−142.21

substituted iodine (I)—human estrogen receptor 2IOK [35].

Conclusions

A novel pyrimidine derivative, 2-chloro-4-(4-fluoro-phenyl)-6-isopropyl-pyrimidine-5-carboxylic acid methyl ester, $C_{20}H_{21}ClO_5$ has been synthesized and purity of the compound has been confirmed by spectroscopic technique. The molecular structure has been investigated by single crystal X-ray diffraction technique. The crystal structure has been stabilized by weak but significant C–H···O, C–H···N, C–F···π and π–π intra and intermolecular hydrogen bond interactions. Ab-initio and Density functional Theory (DFT) calculations have been carried out for the title molecule using RHF/6-311G and B3LYP/6-311G basis set without polarization function respectively. The comparison of the predicted bond lengths and bond angles are in good agreement with experimental results. The Hirshfeld surface analysis and 2D fingerprint map analysis emphasizes that the intermolecular weak but significant interactions C–H···O, C–H···N, C–F···π and π–π hydrogen bonding contributing to the molecular stability. The Hirshfeld surface with finger plot reveals the percentage of intermolecular contacts of the title compound. The docking results show that the good interaction between human estrogen receptor with iodine (I) derivative with energy value of (−142.21) revealing more compatibility with I than the other analogous.

Acknowledgments We are thankful to CSMCRI, Bhavnagar, India for collecting intensity data of the crystal using Smart Apex –II CCD diffractometer.

References

1. Lagoja LM (2005) Chem Biodivers 2(1):1–50
2. Hashash MA, Mahmoud MR, Madboli SA (1993) Indian J Chem B 32:449–451
3. Brunelle MN, Lucifora J, Neyts J, Villet S, Holy A, Trepo C, Zoulim F (2007) Antimicrob Agents Chemother 51:2240
4. Ding Y, Girardet JL, Smith KL, Larson G, Prigaro B, Wu JZ, Yao N (2006) Bioorg Chem 34:26
5. Calabresi P, Parks RE, Goodman LS, Gilman A (1975) The pharmacological basis of therapeutics, 5th edn. Macmillan, New York
6. Safarjalani N, Zhou X, Rais RH, Shi J, Schinazi RF, Naguib FNM, Kouni MH (2005) Cancer Chemother Pharm 55:541
7. Kandeel MM, Mohamed LW, Hamid MAEK, Negmeldin AT (2012) Sci Pharmaceut 80(3):531–545
8. Al-Safarjalani ON, Zhou X, Rais RH, Shi J, Schinazi RF, Naguib FNM, El-Kouni MH (2005) Cancer Chemother Pharm 55:541–551
9. Bruno V, Castaldo A, Centore R, Sirigu A, Sarcinelli F, Casalboni M, Pizzoferrato R (2002) J Polym Sci A Polym Chem 40:1468–1475
10. Castaldo A, Centore R, Peluso A, Sirigu A, Tuzi A (2002) Struct Chem 13:27–36
11. Patel UH, Gandhi SA (2008) Indian J Pure Appl Phys 49:263–269
12. Patel UH, Gandhi SA, Barot VM, Patel MC (2009) Acta Crystallogr E 68:o2926
13. Patel UH, Gandhi SA, Barot VM, Patel MC (2013) Cryst Struct Theory Appl 2:167
14. Patel UH, Gandhi SA, Barot VM, Patel MC (2016) Mol Cryst Liq Cryst 624:190–204
15. Spackman MA, McKinnon JJ (2002) CrystEngComm 4:378–392
16. Fabbiani FPA, Leech CK, Shankland K, Johnston A, Fernandes P, Florence AJ, Shankland N (2007) Acta Crystallogr C63:o659
17. Seth SK, Saha I, Estarellas C, Frontera A, Kar T, Mukhopadhyay S (2011) Cryst Growth Des 11:3250
18. Sheldrick GM (2013) Acta Crystallogr A 64:112–122
19. Sheldrick GM (2015) Acta Crystallogr A 71:3–8
20. Farrugia LJ (2012) J Appl Crystallogr 45:849–854
21. Spek AL (2009) Acta Crystallogr D 65:148–155
22. Becke AD (1993) J Chem Phys 98:1372
23. Jhonson BG, Gill PM, Pople JA (1993) J Chem Phys 98:5612
24. Lee C, Yang W, Parr RG (1988) Phys Rev B 37:785–789
25. Frisch MJ, Trucks GW, Schlegel HB, Scuseria GE, Robb MA, Cheeseman JR, Zakrzewski VG, Montgomery JA, Stratmann RE, Burant JC, Dapprich S, Millam JM, Daniels AD, Kudin KN, Strain MC, Farkas O, Tomasi J, Barone V, Cossi M, Cammi R, Mennucci B, Pomelli C, Adamo C, Clifford S, Ochterski J, Petersson GA, Ayala PY, Cui Q, Morokuma K, Malick DK, Rabuck AD, Raghavachari K, Foresman JB, Cioslowski J, Ortiz JV, Stefanov BB, Liu G, Liashenko A, Piskorz P, Komaromi I, Gomperts R, Martin RL, Fox DJ, Keith T, Al-Laham MA, Peng CY, Nanayakkara A, Gonzalez C, Challacombe M, Gill PMW, Johnson BG, Chen W, Wong MW, Andres JL, Head-Gordon M, Replogle ES, Pople JA (2009) Gaussian 09 Revision A1. Gaussian Inc., Wallingford, CT
26. Dennington R, Keith T, Millam J (2009) Gauss view version 5. Semichem Inc., Shawnee Mission KS
27. Wollf SK, Grimwood DJ, McKinnon JJ, Jayatilaka D, Spackman MA (2007) Crystalexplorer 2.1. University of Western Australia, Perth
28. Clausen HF, Chevallier MS, Spackman MA, Iversen BB (2010) New J Chem 34:193–199
29. Ritchie DW, Venkatraman V (2010) Ultra-fast FFT protein docking on graphics processors. Bioinformatics 26:2398–2405
30. Nardelli M (1995) J Appl Crystallogr 28:659
31. Bernstein J, Davis RE, Shimoni L (1995) Angew Chem Int Edit 34:1555
32. Yılmaz B, Saracoglu H, Caliskan N, Yilmaz I, Cukurovali A (2012) J Chem Crystallogr 42:897–904
33. Kara YS, Sagdinc SG, Karaday N (2013) Spectrochim Acta Part A 110:351–363
34. Namık Ö, Bilge E, Muharrem D, Yunus B (2010) Mol Phys 108:13–24
35. Dhananjaya K, Sibi G, Mallesha H, Ravikumar KR, Awasthi S (2012) Asian Pac J Trop Biomed 2:S1747–S1753